Chemical Physics Letters 731 (2019) 136605

Contents lists available at ScienceDirect

Chemical Physics Letters

journal homepage: www.elsevier.com/locate/cplett

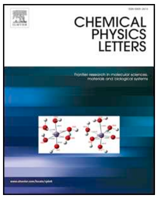

Research paper

The atmospheric impact of the reaction of N_2O with NO_3: A theoretical study

Thanh Lam Nguyen[a], Manolis N. Romanias[b], A.R. Ravishankara[c,1,*], Aristotelis M. Zaras[d,e], Philippe Dagaut[d,e], John F. Stanton[a,*]

[a] *Quantum Theory Project, Department of Chemistry and Physics, University of Florida, Gainesville, FL 32611, USA*
[b] *IMT Lille Douai, Univ. Lille, SAGE – Département Sciences de l'Atmosphère et Génie de l'Environnement, F-59000 Lille, France*
[c] *Departments of Chemistry and Atmospheric Sciences, Colorado State University, Ft. Collins, CO 80523, USA*
[d] *CNRS-INSIS, Institut de Combustion, Aérothermique, Réactivité et Environnement, 1C avenue de la recherche scientifique, 45071 Orléans cedex 2, France*
[e] *Université d'Orléans, 6 avenue du Parc Floral, 45100 Orléans, France*

HIGHLIGHTS

- Nitrous oxide is a greenhouse gas and a potential O_3-depleting substance.
- OH, Cl, and NO_3 do not react fast enough with N_2O.
- These reactions are too slow to be observed experimentally.
- A reaction of NO_3 with N_2O might influence the atmospheric lifetime of N_2O.
- Mechanism and kinetics of the $NO_3 + N_2O$ reaction have been studied for the first time.

ABSTRACT

The reaction of N_2O with NO_3 is studied for the first time using high-level quantum chemical calculations, followed by statistical rate coefficient estimations. Two reaction pathways giving $NO_2 + N_2 + O_2$ and $NO_2 + 2NO$ have been explored. The formation of $NO_2 + N_2 + O_2$ is exothermic by 30 kcal mol^{-1} while that of $NO_2 + 2NO$ is endothermic by 13 kcal mol^{-1}. Both mechanisms have significant reaction barriers, and the reaction rate constants are very low: about 6×10^{-43} cm^3 s^{-1} at 298 K. Therefore, this reaction is not expected to affect the lifetime of N_2O in the atmosphere.

1. Introduction

Nitrous oxide, N_2O, is a major greenhouse gas and its emissions are now the largest of all ozone layer depleting gases [1]. One of the key reasons for these two influences is the long atmospheric lifetime of N_2O (roughly 120 years), which appears not to have any appreciable loss pathway in the troposphere where it is emitted. If there were any reactions in the troposphere that lead to destruction of N_2O, the atmospheric lifetime of this species would be altered even if the reaction were slow. Therefore, a search for potential slow reactions of tropospheric free radicals with N_2O is of interest.

It is not always easy to directly measure the rate coeffcients for very slow radical-molecule reactions due to various experimental difficulties. These include the need to avoid impurity reactions and unwanted side reactions, and the need to use of very large concentrations of N_2O with potential deleterious effects on the ability to detect the radicals. Therefore, assessing the feasibility of slow reactions via theoretical calculations represents an attractive alternative, especially for small molecules. Quantum chemistry calculations have advanced to a stage that it is now fairly straightforward to obtain energetics that are accurate to a few tenths of kcal mol^{-1}. In addition, approaches for calculating rate coefficients using the mapped out potential energy surfaces have advanced. Therefore, we have undertaken a study of the potentially important atmospheric reaction of NO_3 with N_2O. The abundance of NO_3, though highly variable, is sufficiently large that this reaction could have an impact on the lifetime of N_2O if the rate coefficient were of the order of 10^{-20} cm^3 molecule^{-1} s^{-1}, or larger.

Previously, Cantrell et al. [2] attempted to measure this rate coefficient and obtained an upper limit of 2×10^{-17} cm^3 molecule^{-1} s^{-1}. As can be inferred from the preceding, this is not a sufficiently stringent upper limit to dismiss the possibility that this reaction contributes meaningfully to the loss of N_2O in the atmosphere. Therefore, better estimates are needed. A computational estimation of the rate coefficient for the reaction of NO_3 with N_2O is the goal of this focused study.

---

* Corresponding authors at: Quantum Theory Project, Department of Chemistry and Physics, University of Florida, Gainesville, FL 32611, USA.
E-mail addresses: A.R.Ravishankara@colostate.edu (A.R. Ravishankara), johnstanton@ufl.edu (J.F. Stanton).

[1] Also associated with the Le Studium, Advanced Institute for Research, Loire Valley, Orleans, France.

https://doi.org/10.1016/j.cplett.2019.136605
Received 25 May 2019; Received in revised form 8 July 2019; Accepted 12 July 2019

1.1. Quantum chemical calculations

The title reaction involves seven heavy atoms, so high-accuracy HEAT [3–5] calculations would be extremely time consuming; consequently, a compromise is made here. This work is based in part on calculations done with the composite G3B3 method [6], which is a variation of G3 theory [7]. G3B3 [6] uses geometries and harmonic zero-point vibrational corrections obtained at the B3LYP/6-31G(d) level of theory, followed by a series of single-point energy calculations done with methods including QCISD(T)/6-31G(d), MP4/6-31 + G(d), MP4/6-31G(2df,p), and MP2/G3Large in order to estimate the QCISD (T) level at the complete basis set limit. In addition, empirical high-level corrections (HLC) and spin-orbit corrections [6] are also included [7]. It is expected that the G3B3 calculations provide (roughly) chemical accuracy (i.e., within 1–2 kcal mol^{-1}) for relative energies. As can be seen in Fig. 1, such a level of accuracy is indeed achieved for the reaction enthalpies of two main pathways, and it is expected that this accuracy will not be seriously degraded for transition state (TS) structures. Moreover, intrinsic reaction coordinate (IRC) [8–10] calculations were also performed in order to verify that the located transition state structures properly connect reactant(s) and products. It should be mentioned that NO_3 is a notoriously difficult molecule for both experiments and theory. DFT calculations with B3LYP give a C_{2v} equilibrium geometry for NO_3, although the experimentally determined ground state average geometry is D_{3h}. Although a comparison of equilibrium geometries with experimental structures is fraught with difficulties, especially for a system of this type, it is true that the potential surface for NO_3 near the minimum is extremely flat. Hence, many methods give symmetric structures while many others give broken symmetry structures. However, the energetics are largely insensitive, owing to the flatness of the potential. The G3B3 and IRC calculations were done using the Gaussian 09 program suite [11].

In addition to the G3B3 calculations, we have also used high-level coupled-cluster calculations to characterize key stationary points (see Fig. 1) for the purpose of chemical kinetics analysis. First, geometries were optimized using the coupled-cluster method with single, double, and perturbative triple excitations (CCSD(T)) [12–14] in combination with the atomic natural orbital double-zeta (ANO0) basis set [15,16], followed by harmonic vibrational analyses in order to check if they are real minima or first-order saddle points. Second, the ANO0 geometries and Hessian matrix obtained above were used for reoptimizing with a larger triple-zeta (ANO1) basis set [15,16]. Third, single-point energies were refined using the same CCSD(T) method, but with Dunning's quadruple-zeta basis set [17], cc-pVQZ. Finally, additional minor corrections have been applied for the effects of scalar relativity, the diagonal Born-Oppenheimer correction (DBOC), and spin-orbit coupling. As can be seen in Fig. 1, both the simple G3B3 and more elaborate CCSD (T)/cc-pVQZ calculations agree well (within 1–2 kcal mol^{-1}) with one another, although the CCSD(T) values are systematically about 1–2 kcal mol^{-1} lower. A similar difference has been found in the reaction of OH with N_2O [18]. All CCSD(T) calculations are done using the CFOUR quantum chemistry package [19].

1.2. Reaction mechanisms and energetics

Two pathways have been characterized for the thermal reaction of NO_3 radical with N_2O (with the reaction enthalpies obtained from published data (ref. [20])). The first:

$$NO_3 + N_2O \rightarrow NO_2 + N_2 + O_2; \quad \Delta_rH \ \ (0\,K) = \ \ -30.7\,kcal\,mol^{-1}(\text{ref. } [20]) \tag{1}$$

(hereafter defined as pathway 1) is very exothermic [20], and leads to the formation of three stable molecules, NO_2, N_2 and O_2. The second pathway (hereafter defined as pathway 2)

$$NO_3 + N_2O \rightarrow NO_2 + 2NO; \ \Delta_rH\ (0\,K) = +12.6\,kcal\,mol^{-1}(\text{ref. } [20]) \tag{2}$$

is endothermic [20], resulting in NO_2 + 2NO, and therefore is highly unlikely to occur under atmospheric conditions. The G3B3 calculations give −29.9 and 12.9 kcal mol^{-1} for reactions (1) and (2), respectively, which agree within 1 kcal mol^{-1} with both the CCSD(T) calculations and well established thermochemical values [20]. The optimized geometries of various species are given in the supplementary material, while those of key transition states and intermediates along the reaction coordinate obtained with the DFT-B3LYP method are shown in Fig. 1. The calculated relative energies including zero-point energy corrections

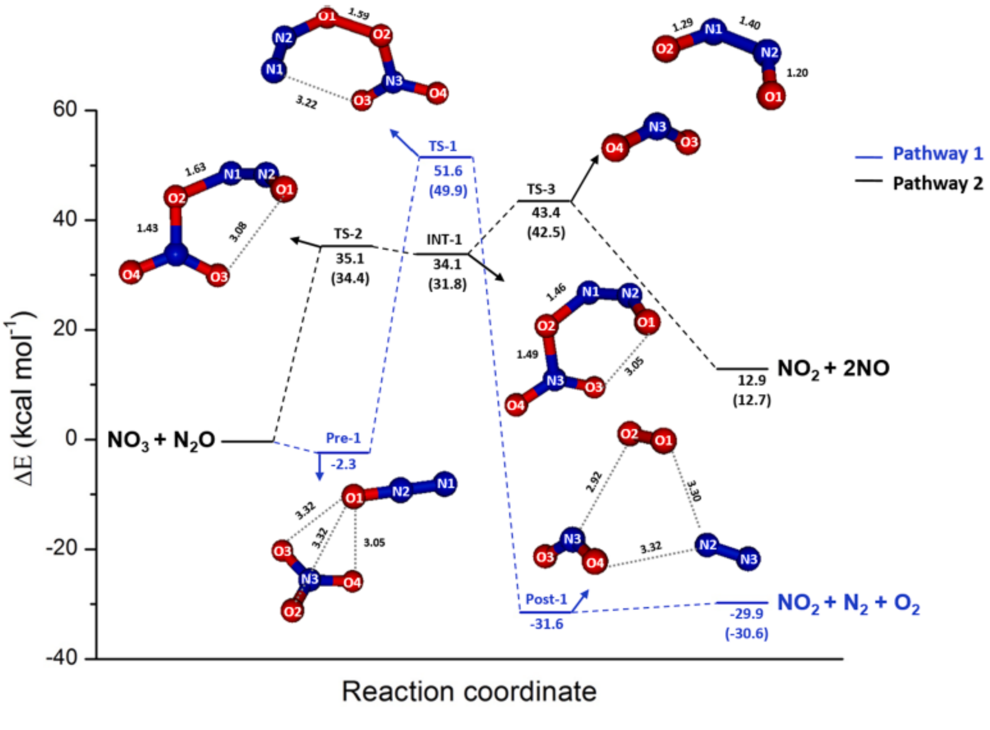

Fig. 1. The potential energy surface for the reaction of NO_3 radical with N_2O calculated using the G3B3 method. The energy values given in parenthesis are obtained at the CCSD(T)/cc-pVQZ level of theory. The black and blue lines correspond to the endothermic and exothermic pathways respectively. The bond lengths are given in Å. (For interpretation of the references to colour in this figure legend, the reader is referred to the web version of this article.)

Table 1
Calculated relative energies (kcal mol^{-1}) of various species involved in the reaction of NO_3 with N_2O for the exothermic and endothermic channels.

$NO_3 + N_2O \rightarrow NO_2 + N_2 + O_2$			$NO_3 + N_2O \rightarrow NO_2 + 2NO$		
Species	G3B3	CCSD(T)/cc-pVQZ	Species	G3B3	CCSD(T)/cc-pVQZ
Pre-1	−2.3	n/a	TS-2	35.1	34.4
TS-1	51.6	49.9	INT1	34.1	31.8
Post-1	−31.6	n/a	TS-3	43.4	42.5
$NO_2 + N_2 + O_2$	−29.9 (−30.72 ± 0.1) [a]	−30.6 (−30.72 ± 0.1) [a]	NO_2 + 2NO	12.9 (12.60 ± 0.1) [a]	12.7 (12.60 ± 0.1) [a]

[a] Taken from ATcT, version 1.122d, 2019 [31].

for various species are given in Table 1.

For pathway 1 as presented in Fig. 1, NO_3 attacks the oxygen end of N_2O. Initially, a weakly bound pre-reactive complex is formed (Pre-1) with a binding energy of −2.3 kcal mol^{-1} as calculated with G3B3. This complex then proceeds to abstract an O atom through TS-1 leading to Post-1. The barrier height of TS-1 is calculated to be 51.6 and 49.9 kcal mol^{-1} using the G3B3 and CCSD(T) methods, respectively. Post-1, a post-reaction complex with a relative energy of −31.6 kcal mol^{-1}, when produced, should rapidly dissociate at temperatures relevant to the atmosphere to the final products, $NO_2 + N_2 + O_2$ driven by the very large entropy increase, together with a negligible barrier and low endothermicity (~1 kcal mol^{-1}). According to Fig. 1, TS-1 is the key saddle point, because passing over (or through) TS-1 is the rate-determining step. Yet, TS-1 has a large spin contamination ($< S^2 >$) of 1.5. So, in addition to UHF-CCSD(T) method, ROHF-CCSD(T) was also used for optimization. A comparison of two optimized geometries are displayed in Fig. 2 with the ROHF-CCSD(T) values shown in parentheses. Inspection of Fig. 2 shows that the two geometries are in good agreement: there are small differences of 0.015 Å for the O—O bond length and of 0.4 degrees for the ∠NOO angle. However, there is a difference of 2 kcal mol^{-1} (not shown in Fig. 1) for the calculated barrier heights, where the ROHF-CCSD(T) method gives a lower value. Because of this, we take the 49.9 kcal mol^{-1} barrier height from ROHF-CCSD(T)/cc-pVQZ, but recognize that it is associated with a relatively large uncertainty (up to perhaps 3–5 kcal mol^{-1}).

For pathway 2 as displayed in Fig. 1, NO_3 can attack the nitrogen end of N_2O via TS-2 leading to the formation of an intermediate adduct, INT1. The energy barrier of TS-2 is calculated to be 35.1 and 34.4 kcal mol^{-1} using the G3B3 and UHF-CCSD(T) methods, respectively. INT1 lies a few kcal mol^{-1} lower than TS-2. There are two possible pathways starting at INT1: it either dissociates via TS-2 back to the initial reactants, $NO_3 + N_2O$, or decomposes further via TS-3 to give products, NO_2 + 2NO. Given that the redissociation step faces a much lower barrier, it is expected to be dominant. As a result, the rate-determining step in this scenario is to surmount TS-3.

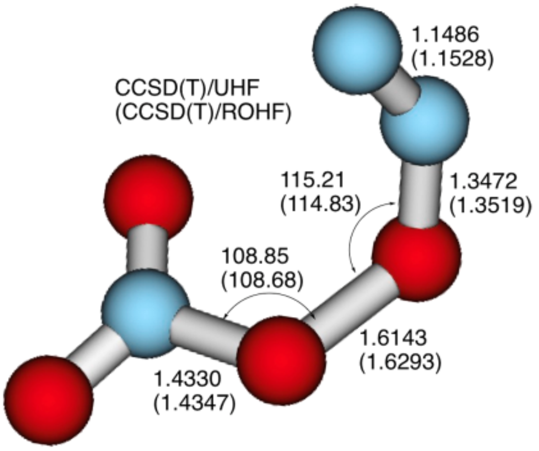

Fig. 2. Geometrical parameters of TS-1 are optimized using UHF-CCSD(T)/ANO1 and ROHF-CCSD(T)/ANO1 (parenthesis) levels of theory. The energy at the ROHF-CCSD(T)/ANO1 level of theory is 2 kcal mol^{-1} lower than that of the other.

1.3. Statistical rate coefficient calculations

Pathway 1: $NO_3 + N_2O \rightarrow TS\text{-}1 \rightarrow NO_2 + N_2 + O_2$

As seen in Fig. 1, when formed from the association of NO_3 with N_2O, Pre-1 rapidly re-dissociates back to reactants because the subsequent O-abstraction step must overcome a very high barrier. As a result, the canonical equilibrium, $NO_3 + N_2O \rightleftharpoons$ Pre-1, is quickly established before the following O-abstraction can occur. In addition, Post-1 – as produced by passing over TS-1 – has substantial internal energy, and thus rapidly decomposes to products, $NO_2 + N_2 + O_2$. Because of this, the influences of Pre-1 and Post-1 on kinetics of the reaction are negligible (for example, it makes a difference of less than 5% at any atmospheric relevant temperature, see the Supplementary Material). Consequently, a kinetics scheme in this scenario can be simplified to: $NO_3 + N_2O \rightarrow TS\text{-}1 \rightarrow NO_2 + N_2 + O_2$, which does not go through a long-lived intermediate, and therefore is expected to be pressure-independent. Thermal rate constants can be calculated using transition state theory (TST) [21,22] at the high-pressure limit:

$$k_{TST}(T) = \frac{\sigma}{h} \times \frac{Q_{tr}^{\neq} Q_{e}^{\neq}}{Q_{NO_3}^{re} \cdot Q_{N_2O}^{re}} \times \sum_{J=0}^{\infty} (2J+1) \int_0^{\infty} G_{rv}^{\neq}(E, J) \exp(-E/k_B T) dE \tag{3}$$

where h is Planck's constant, k_B is Boltzmann's constant, and $\sigma = 12$ is the reaction path degeneracy. For the latter, note that rotational symmetry numbers are 6, 1, and 1, respectively, for NO_3, N_2O, and TS-1. In addition, TS-1 is chiral and therefore has a mirror image. $Q_{NO_3}^{re}$ and $Q_{N_2O}^{re}$ are the complete partition functions for NO_3 and N_2O, respectively. Q_{tr} is the translational partition function and Q_e is the electronic partition function (the superscripts "re" and "≠" designate reactants and transition state, respectively). J is the total angular momentum quantum number. $G_{rv}^{\neq}$ is the sum of rovibrational states for TS-1 obtained by convoluting vibrational and rotational quantum states [23]:

$$G_{rv}^{\neq}(E, J) = \int_0^{E} G_{v}^{\neq}(E - E_r) \rho_r^{\neq}(E_r) dE_r \tag{4}$$

where $\rho_r^{\neq}(E_r)$ is the density of states at energy E_r. It is assumed that all stationary points on the potential energy surface are approximated by a rigid-rotor symmetric top [23], for which rotational energy levels are given by Eq. (5):

$$E_r(J, K) = J(J+1)\bar{B} + (A - \bar{B})K^2, \text{ with } \bar{B} = \sqrt{B \cdot C} \text{ and } -J \le K \le +J \tag{5}$$

With A, B, and C as the rotational constants. It should be mentioned that tunneling effects with an asymmetric Eckart model [24] are included in computing $G_v^{\neq}$in Eq. (4) through Eq. (6) [25]:

Table 2
Calculated thermal rate constants ($cm^3\,molecule^{-1}\,s^{-1}$) and tunneling corrections for the direct O-abstraction pathway 1: $NO_3 + N_2O \rightarrow N_2 + NO_2 + O_2$.

T (K)	CTST	CTST/Eckart	Tunneling correction
100	2.82×10^{-121}	6.04×10^{-102}	2.15×10^{19}
125	1.81×10^{-99}	4.94×10^{-87}	2.73×10^{12}
150	6.54×10^{-93}	5.38×10^{-85}	8.23×10^{7}
175	1.70×10^{-74}	1.10×10^{-69}	6.48×10^{4}
200	1.14×10^{-66}	6.14×10^{-64}	538
225	1.44×10^{-60}	5.16×10^{-59}	35.9
250	1.12×10^{-55}	1.14×10^{-54}	10.2
275	1.15×10^{-51}	6.20×10^{-51}	5.41
300	2.58×10^{-48}	9.56×10^{-48}	3.72
325	1.79×10^{-45}	5.18×10^{-45}	2.89
350	4.96×10^{-43}	1.20×10^{-42}	2.42
375	6.56×10^{-41}	1.39×10^{-40}	2.12
400	4.78×10^{-39}	9.10×10^{-39}	1.91

$$G_v^{\neq}(E) = \int_0^E P(x)_{Eckart} \times \rho_v^{\neq}(E - x)dx \tag{6}$$

Here P(x) is the asymmetric Eckart tunneling probability.

The rate constants calculated as a function of temperature are shown in Table 2. Inspection of Table 2 shows that k(T) increases sharply by about *sixty-three orders of magnitude* when temperature rises from 100 to 400 K, as expected for a reaction having a high reaction barrier. Because of the motion of the heavy oxygen atom, the tunneling correction also increases significantly with decreasing temperature: it is a factor of *ca.* 4 at 300 K and becomes about 2×10^{19} at 100 K; but, even such a large tunneling enhancement is insufficient to overcome the very small rate constant caused by the high barrier. At room temperature, the calculated rate constant is $1 \times 10^{-47}\,cm^3\,molecule^{-1}\,s^{-1}$, which corresponds to a N_2O lifetime of 2×10^{38} s (about 10^{31} years), assuming an atmospheric $[NO_3] \approx 5 \times 10^8\,molecules/cm^3$ [26]. Note that the globally averaged NO_3 abundance is ill-defined and would be much smaller. Even if this rate coefficient were ten orders of magnitude larger, it would not make any contribution to the atmospheric removal of N_2O. At the lower temperatures, the rate coefficient will be even smaller. Therefore (even allowing for considerable uncertainty in our calculations), it can be safely concluded that reaction pathway 1 has absolutely no relevance in the atmosphere; it is most certainly not a potential sink for N_2O.

Pathway 2: $NO_3 + N_2O \rightarrow TS\text{-}2 \rightarrow INT1 \rightarrow TS\text{-}3 \rightarrow NO_2 + 2NO$

As shown in Fig. 1, the endothermic reaction pathway 2 to form $NO_2 + 2NO$ from $NO_3 + N_2O$ passes through an intermediate INT1, which does not have a long lifetime. Therefore, this pathway may depend on pressure. If it does, a master equation analysis is required to compute rate constants as functions of both temperature and pressure. To check this idea, we have computed thermal rate constants at two extreme conditions: the low- and high-pressure limits where analytical solutions can be obtained through Eq. (7) and Eq. (8), respectively.

At the low-P limit [27,28]:

$$k(T)_{P=0} = \frac{\sigma}{h} \times \frac{Q_{tr}^{\neq} Q_e^{\neq}}{Q_{NO_3}^{re} \cdot Q_{N_2O}^{re}} \times \sum_{J=0}^{\infty} (2J + 1) \int_0^{\infty} G_{eff}^{\neq}(E, J)\exp(-E/k_BT)dE \tag{7a}$$

Here $G_{eff}^{\neq}$ is the effective sum of rovibrational quantum states, which is given by Eq. (7b):

$$G_{eff}^{\neq} = \frac{G_{TS2}^{\neq}(E, J) \times G_{TS3}^{\neq}(E, J)}{G_{TS2}^{\neq}(E, J) + G_{TS3}^{\neq}(E, J)} \tag{7b}$$

At the high-P limit [28]:

$$k(T)_{P=\infty} = \frac{k_2(T) \times k_3(T)}{k_{-2}(T) + k_3(T)} \tag{8}$$

Table 3
Calculated individual thermal rate constants (in the reaction pathway 2) at the high-pressure limit.

T (K)	$k_2(T)$ in $cm^3\,molecule^{-1}\,s^{-1}$	$k_{-2}(T)$ in s^{-1}	$k_3(T)$ in s^{-1}
100	3.38×10^{-86}	4.89×10^{6}	3.84×10^{-7}
125	1.09×10^{-71}	2.07×10^{7}	1.60×10^{-5}
150	6.32×10^{-62}	6.44×10^{7}	8.56×10^{-4}
175	6.62×10^{-55}	1.56×10^{8}	3.59×10^{-2}
200	1.30×10^{-49}	3.14×10^{8}	8.45×10^{-1}
225	1.77×10^{-45}	5.51×10^{8}	1.13×10^{1}
250	3.70×10^{-42}	8.70×10^{8}	9.63×10^{1}
275	1.97×10^{-39}	1.27×10^{9}	5.74×10^{2}
300	3.76×10^{-37}	1.75×10^{9}	2.59×10^{3}
325	3.24×10^{-35}	2.29×10^{9}	9.38×10^{3}
350	1.50×10^{-33}	2.89×10^{9}	2.85×10^{4}
375	4.20×10^{-32}	3.52×10^{9}	7.49×10^{4}
400	7.86×10^{-31}	4.20×10^{9}	1.75×10^{5}

where $k_2(T)$ is the thermal rate constant for the forward step: $NO_3 + N_2O \rightarrow TS\text{-}2 \rightarrow INT1$, $k_{-2}(T)$ is the thermal rate constant for the reverse process: $INT1 \rightarrow TS\text{-}2 \rightarrow NO_3 + N_2O$, and $k_3(T)$ is the thermal rate constant for the formation of the products: $INT1 \rightarrow TS\text{-}3 \rightarrow NO_2 + 2NO$.

These three rate constants are computed using TST and presented in Table 3. Inspection of Table 3 shows that the loss of INT1 through TS-2 is many orders of magnitude faster than via TS-3, so that INT1 rapidly re-dissociates back to the initial reactants once it is produced. Consequently, INT1 has a very short lifetime that is not compatible with thermalization via collisions with a third body such as N_2 (and/or O_2) under atmospheric conditions. In other words, this reaction pathway is pressure-independent (also supported by the numbers in Table 4 where the difference between the low- and high-pressure rate constants is much smaller than 1%).

Comparison of the rate coefficient calculated at 298 K with the only reported value is useful. Cantrell et al. [2] measured the rate coefficient at P = 1 atm in air. Their reported upper limit is consistent with our calculations, but it is to be noted that our value is many orders of magnitude smaller than their upper limit.

Inspection of Table 4 shows that the calculated rate constants increase with temperature, as expected for a reaction having a high barrier. At room temperature, we obtain a rate constant of *ca.* $6 \times 10^{-43}\,cm^3\,molecule^{-1}\,s^{-1}$ which, although five orders of magnitude faster than pathway 1, still leads to a calculated atmospheric lifetime of N_2O of *ca.* $\sim 3 \times 10^{33}$ s ($> 10^{26}$ years). Thus, taken together with our results for Reaction (1), the contribution of NO_3 reacting with N_2O to

Table 4
. Calculated rate constants ($cm^3\,molecule^{-1}\,s^{-1}$) at the low- and high-pressure limits for the addition/elimination reaction pathway 2: $NO_3 + N_2O \rightarrow O_2NONNO \rightarrow NO_2 + 2NO$.

T (K)	Low-P limit [a)]	High-P limit [b)]	diff. (%) [c)]
100	2.6460×10^{-99}	2.6460×10^{-99}	0
125	8.4208×10^{-84}	8.4208×10^{-84}	0
150	8.4022×10^{-73}	8.4022×10^{-73}	0
175	1.5226×10^{-64}	1.5226×10^{-64}	0
200	3.4888×10^{-58}	3.4894×10^{-58}	1.33×10^{-2}
225	3.6344×10^{-53}	3.6354×10^{-53}	2.48×10^{-2}
250	4.0874×10^{-49}	4.0890×10^{-49}	4.09×10^{-2}
275	8.8806×10^{-46}	8.8862×10^{-46}	6.23×10^{-2}
300	5.5558×10^{-43}	5.5616×10^{-43}	8.99×10^{-2}
325	1.3233×10^{-40}	1.3269×10^{-40}	1.25×10^{-1}
350	1.4762×10^{-38}	1.4787×10^{-38}	1.67×10^{-1}
375	8.9186×10^{-37}	8.9380×10^{-37}	2.18×10^{-1}
400	3.2716×10^{-35}	3.2808×10^{-35}	2.78×10^{-1}

[a)] Eq. (5) in the main text.
[b)] Eq. (6) in the main text.
[c)] Difference (%) = $[k(T,P = \infty) - k(T,P = 0)] \times 100\%/k(T,P = \infty)$

the lifetime of N_2O in the atmosphere is completely negligible. Even local influences of NO_3 on N_2O, and vice-versa, would be negligible. At lower atmospheric temperatures, the loss rate would be even smaller. It is of importance to compare the impact of NO_3 on the lifetime of N_2O with that of OH (ref. [18]). As reported previously [18], at room temperature the pseudo first-order reaction rate constant of N_2O with OH is predicted to be about 7×10^{-22} s^{-1}, which is about 10^{12} times faster than the title reaction. So, it can be concluded that the influence of NO_3 is entirely negligible.

It is worth noting that our calculated thermal rate constants may be in error by a few orders of magnitudes due to numerous possible errors in our kinetics calculations that involve barrier heights, RRHO model, tunneling corrections, and so on. Yet, the main conclusion obtained from this study is that the loss of N_2O through either pathway 1 or pathway 2 is utterly negligible in Earth's atmosphere or even on a geological timescale.

2. Discussion

As stated in the introduction, N_2O is one of the most important greenhouse gases, trailing only CO_2 and CH_4 in importance, and is believed to be the most important ozone-depleting substance emission of the 21st Century [1]. Its concentration in the atmosphere has risen steadily in modern times (a roughly linear rise of *ca.* 0.8 ppb yr^{-1} (since 1980 [29]), which has been attributed in large part to an increase in food production. If steps are not made to mitigate its anthropogenic sources (it also has natural sources), its importance as an atmospheric constituent will continue to increase. While it is known that N_2O can be destroyed by photolysis and via reaction with $O(^1D)$ atoms in the upper atmosphere – the modeling of which leads to its estimated atmospheric lifetime of 114 years [30] – other chemical sinks for the molecule are unknown. Accordingly, this is the second in a series of studies that investigate "slow" reactions of N_2O, done with an eye towards discovering potential chemical sinks that are relevant on a time scale of centuries to perhaps millenia. And this is also the second study to investigate a plausible reaction (the first being reaction of N_2O with the hydroxyl radical, OH [18]) to find that N_2O is exquisitely unreactive; atmospheric lifetimes found so far are so long that they are several orders of magnitude greater than that of the universe itself.

It seems likely that N_2O is resistant to all potential chemical loss mechanisms in the atmosphere (apart from reaction with $O(^1D)$ in the stratosphere), and that it is simply a highly unreactive atmospheric molecule like CO_2. One could rationalize this by recognizing that it is isoelectronic with CO_2; decomposition reactions of the latter will lead to the most stable diatomic molecule (CO) while those of nitrous oxide lead to the second most stable diatomic molecule (N_2). Hence, the fact that both molecules lack chemical sinks in the troposphere is not particularly surprising; the consequence of such a situation is that N_2O will continue to grow in importance as a greenhouse gas, and is a molecule that is "*here to stay*".

3. Conclusions

Since it is very difficult to measure very slow free radical reactions, in this work we have estimated the rate coefficient for the potential reaction of NO_3 with N_2O using high-level quantum chemical and statistical chemical kinetics calculations. We find that there are potentially two reaction pathways, both of which have substantial barriers. The following kinetics analysis shows that these reactions are extremely slow and negligible in Earth's atmosphere. It should be noted that uncertainties of even 5 kcal mol^{-1} do not alter the conclusions regarding the loss of N_2O from the troposphere since the upper limits for the rate coeffients are so small.

Declaration of Competing Interest

Author declares that there is no conflicts of interest.

Acknowledgements

The work at University of Florida was supported by the U.S. National Science Foundation (Grant CHE-1664325) and Department of Energy, Office of Science, Office of Basic Energy Sciences under Award DE-FG02-07ER15884. Work of ARR was supported by Colorado State University and Le Studium Advanced Institute for Research, Loire Valley, Orleans, France. We would also like to express our gratitude to an anonymous reviewer for his/her useful comments that improved the quality of this paper.

Appendix A. Supplementary material

Supplementary data to this article can be found online at https://doi.org/10.1016/j.cplett.2019.136605. Theoretical methods, optimized geometries, and rovibrational parameters for various stationary points are provided.

References

[1] A.R. Ravishankara, J.S. Daniel, R.W. Portmann, Nitrous oxide (N2O): the dominant ozone-depleting substance emitted in the 21st century, Science 326 (2009) 123–125.
[2] C.A. Cantrell, J.A. Davidson, R.E. Shetter, B.A. Anderson, J.G. Calvert, Reactions of nitrate radical and nitrogen oxide (N2O5) with molecular species of possible atmospheric interest, J. Phys. Chem. 91 (1987) 6017–6021.
[3] A. Tajti, P.G. Szalay, A.G. Csaszar, M. Kallay, J. Gauss, E.F. Valeev, B.A. Flowers, J. Vazquez, J.F. Stanton, HEAT: high accuracy extrapolated ab initio thermochemistry, J. Chem. Phys. 121 (2004) 11599–11613.
[4] Y.J. Bomble, J. Vazquez, M. Kallay, C. Michauk, P.G. Szalay, A.G. Csaszar, J. Gauss, J.F. Stanton, High-accuracy extrapolated ab initio thermochemistry. II. Minor improvements to the protocol and a vital simplification, J. Chem. Phys. 125 (2006).
[5] M.E. Harding, J. Vazquez, B. Ruscic, A.K. Wilson, J. Gauss, J.F. Stanton, High-accuracy extrapolated ab initio thermochemistry. III. Additional improvements and overview, J. Chem. Phys. 128 (2008).
[6] A.G. Baboul, L.A. Curtiss, P.C. Redfern, K. Raghavachari, Gaussian-3 theory using density functional geometries and zero-point energies, J. Chem. Phys. 110 (1999) 7650–7657.
[7] L.A. Curtiss, K. Raghavachari, P.C. Redfern, A.G. Baboul, J.A. Pople, Gaussian-3 theory using coupled cluster energies, Chem. Phys. Lett. 314 (1999) 101–107.
[8] K. Fukui, The path of chemical-reactions - the irc approach, Acc. Chem. Res. 14 (1981) 363–368.
[9] H.P. Hratchian, H.B. Schlegel, Accurate reaction paths using a Hessian based predictor-corrector integrator, J. Chem. Phys. 120 (2004) 9918–9924.
[10] H.P. Hratchian, H.B. Schlegel, Using Hessian updating to increase the efficiency of a Hessian based predictor-corrector reaction path following method, J. Chem. Theory Comput. 1 (2005) 61–69.
[11] M.J. Frish, G.W. Trucks, H.B. Schlegel, G.E. Scuseria, M.A. Robb, e. al., Gaussian 09, Revision D.01, In Wallingford CT, 2009.
[12] J.F. Stanton, Why CCSD(T) works: a different perspective, Chem. Phys. Lett. 281 (1997) 130–134.
[13] K. Raghavachari, G.W. Trucks, J.A. Pople, M. Headgordon, A 5th-order perturbation comparison of electron correlation theories, Chem. Phys. Lett. 157 (1989) 479–483.
[14] R.J. Bartlett, J.D. Watts, S.A. Kucharski, J. Noga, Noniterative 5th-order triple and quadruple excitation-energy corrections in correlated methods, Chem. Phys. Lett. 165 (1990) 513–522.
[15] J. Almlof, P.R. Taylor, General contraction of gaussian-basis sets. 1. Atomic natural orbitals for 1st-row and 2nd-row atoms, J. Chem. Phys. 86 (1987) 4070–4077.
[16] J. Almlof, P.R. Taylor, General contraction of gaussian-basis sets. 2. Atomic natural orbitals and the calculation of atomic and molecular-properties, J. Chem. Phys. 92 (1990) 551–560.
[17] T.H. Dunning, Gaussian-basis sets for use in correlated molecular calculations. 1. The atoms boron through neon and hydrogen, J. Chem. Phys. 90 (1989) 1007–1023.
[18] T.L. Nguyen, A.R. Ravishankara, J.F. Stanton, Analysis of the potential atmospheric impact of the reaction of N2O with OH, Chem. Phys. Lett. 708 (2018) 100–105.
[19] J.F. Stanton, e. al., CFOUR, a quantum chemical program package, For the current version, see http://www.cfour.de.
[20] S.P. Sander, R.R. Friedl, J.R. Barker, D.M. Golden, M.J. Kurylo, P.H. Wine, J.P.D. Abbatt, J.B. Burkholder, C.E. Kolb, G.K. Moorgat, R.E. Huie, V.L. Orkin, JPL Evaluation number 17: Chemical Kinetics and Photochemical Data for Use in Atmospheric Studies; 2011.
[21] H. Eyring, The activated complex in chemical reactions, J. Chem. Phys. 3 (1935) 107–115.

[22] M.G. Evans, M. Polanyi, Some applications of the transition state method to the calculation of reaction velocities, especially in solution, Trans. Faraday Soc. 31 (1935) 0875–0893.
[23] T. Baer, W.L. Hase, Unimolecular reaction dynamics : theory and experiments, Oxford University Press, New York, 1996.
[24] W.H. Miller, Tunneling corrections to unimolecular rate constants, with application to formaldehyde, J. Am. Chem. Soc. 101 (1979) 6810–6814.
[25] W. Forst, Unimolecular reactions : a concise introduction, Cambridge University Press, Cambridge, U.K. ; New York, 2003.
[26] R. Atkinson, Gas-phase tropospheric chemistry of volatile organic compounds: 1. Alkanes and alkenes, J. Phys. Chem. Ref. Data 26 (1997) 215–290.
[27] W.H. Miller, Unified statistical-model for complex and direct reaction-mechanisms, J. Chem. Phys. 65 (1976) 2216–2223.
[28] T.L. Nguyen, B.C. Xue, R.E. Weston, J.R. Barker, J.F. Stanton, Reaction of HO with CO: tunneling is indeed important, J. Phys. Chem. Lett. 3 (2012) 1549–1553.
[29] T.M. Thompson, Halocarbons and other atmospheric trace, species. In: Climate Monitoring and Diagnostics Laboratory, Summary, Report No. 27 [Schnell, R.C., A.-M. Buggle, and R.M. Rosson (eds.)].NOAA CMDL, Boulder, CO, pp. 115–135; 2004.
[30] S.A. Montzka, Controlled substances and other source gases. In: Scientific Assessment of Ozone Depletion: 2002. World Meteorological Organization, Geneva, pp. 1.1–1.83; 2003.
[31] B. Ruscic, D.H. Bross, Active Thermochemical Tables (ATcT) values based on ver. 1.122d of the Thermochemical Network (2018), available at ATcT.anl.gov, 2018.